JOURNAL OF GEOPHYSICAL RESEARCH, VOL. 89, NO. C3, PAGES 3689-3704, MAY 20, 1984

A MODEL FUNCTION FOR OCEAN RADAR CROSS SECTIONS AT 14.6 GHz

F. J. Wentz

Remote Sensing Systems

S. Peteherych

Meteorological Services Research Branch, Atmospheric Environment Service

L. A. Thomas

Remote Sensing Systems

Abstract. The relationship between the ocean's normalized radar cross section (NRCS) at 14.6 GHz and the surface wind vector is derived using the 3 months of Seasat microwave scatterometer (SASS) measurements. The derivation is based on the statistics of the SASS observations, and no in situ measurements are required, other than a mean global wind speed, which comes from climatology. The frequency distribution of the global wind vectors observed by SASS is assumed to be a bivariate normal probability function. A NRCS model function is found that maps the assumed wind vector statistics into the observed SASS NRCS statistics. This function is compared with a NRCS model coming from the Joint Air Sea Interaction Experiment (JASIN) and with aircraft scatterometer measurements. The results indicate that the statistically derived NRCS model is an improvement over the JASIN model, which was based on a limited number of in situ anemometer measurements.

1. Introduction

The relationship between the ocean's radar cross section and wind has been under investigation for several decades. The early experiments revealed a strong correlation between the normalized radar cross section (NRCS) and the surface wind speed W [Cowan, 1946; Kerr, 1951; Grant and Yapley, 1957]. During the 1960's and 1970's, the Naval Research Laboratory (NRL) [Guinard et al., 1971; Daley, 1973] and NASA Langley Research Center [Jones and Schroeder, 1978] flew many aircraft scatterometer missions to quantify the NRCS versus wind relationship. At first, the NRL data seemed to show a weak NRCS versus wind speed dependence. However, a reanalysis of the NRL data [Claassen et al., 1972] showed a stronger wind dependence, which was consistent with the results coming from the Langley AAFE RADSCAT experiments. The first satellite scatterometer experiment was conducted aboard Skylab in 1973, using the S-193 RADSCAT [Young and Moore, 1977]. The basic conclusion coming from these various experiments was that the NRCS increases as a power of wind speed and varies with wind direction as the cosine of 2χ, where χ is the observation azimuth angle relative to the wind direction.

Paper number 3C1884.
0148-0227/84/003C-1884$05.00

The launch of the Seasat 14.6 GHz scatterometer (SASS) in 1978 began a significant advancement in understanding radar backscattering from the ocean. For the first time, the NRCS of the world's oceans were systematically measured by a stable-gain scatterometer. During the 3-month life of Seasat, SASS took 20 million radar observations of the ocean surface, which were archived on magnetic tape. The first utilization of the SASS data was to better define the NRCS versus wind vector relationship (i.e., the NRCS model function). The approach was to compare the wind vectors coming from the original SASS geophysical algorithm with wind fields generated from in situ anemometer measurements. The original algorithm utilized a model function derived from the Langley RADSCAT aircraft measurements [Wentz, 1977]. The in situ winds came from two oceanographic experiments: the Gulf of Alaska Seasat Experiment (GOASEX) and the Joint Air Sea Interaction Experiment (JASIN) [Brown et al., 1982], with JASIN receiving the most emphasis. Statistics on the so-called error between the SASS wind and the in situ wind were generated and stratified according to polarization, incidence angle, and wind speed. The NRCS model function was then modified so as to eliminate any biases between the SASS winds and in situ winds [Jones et al., 1982; Schroeder et al., 1982].

There are a number of drawbacks to the JASIN derivation of the model function. First, the in situ wind fields are subject to error. Although Brown et al. [1982] estimate the JASIN fields are in error by ± 1 m/s, Weller et al. [1983] indicate that the actual error is larger due to problems with the buoy anemometers and that the reference anemometer W2/VAWR is biased high by 10%. Additional errors in the in situ wind fields will result from unknown mesoscale turbulence. The second problem is the small number of observations. For a given polarization, 5° incidence angle stratification, and 2 m/s wind speed stratification, there are typically only 7 JASIN comparisons between the SASS wind and the field wind. The problem is compounded by the fact that the comparisons are not always independent in that the same wind field is used in different comparisons. Finally, the derivation was not subject to any physical or statistical restraints. The degrees of freedom in tuning the model function were much greater than the number of observations. For example, when an error was

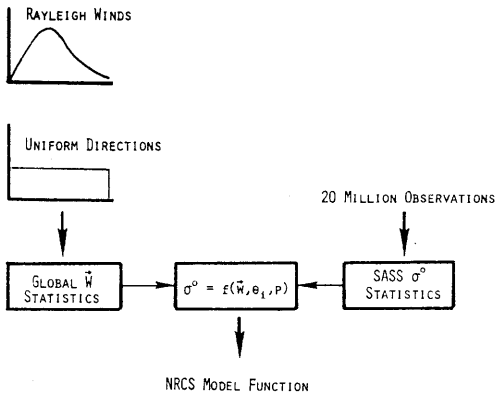

Fig. 1. Derivation of NRCS model function.

detected for a particular polarization, incidence angle, and wind speed, the corresponding entry in the model function table was changed so as to eliminate the error. This NRCS table, which is called the GH Table, has a total of 1596 entries that may be adjusted.

We consider SASS to be a highly accurate spaceborne anemometer capable of measuring synoptic and mesoscale wind field features better than conventional anemometers. In view of this and the problems with the JASIN tuning, we began investigating ways to derive the NRCS model function without resorting to in situ anemometers. Our approach is depicted in Figure 1. The frequency distribution of the wind speed at a 50-km resolution over the globe for the 3-month Seasat period is assumed to be a Rayleigh distribution, and the distribution of the wind direction relative to the SASS antennas is taken to be a uniform distribution. Statistics on the means and variances of the 20 million SASS NRCS measurements are computed and stratified according to polarization and incidence angle. The problem is to then find a function that will map the wind speed and direction statistics into the observed NRCS statistics. To do this, we use a simple model that relates the NRCS to polarization, incidence angle, wind speed, and relative azimuth angle. The model has six parameters, each of which depends on polarization and incidence angle. We find values for the parameters so that the model produces the observed NRCS statistics given as input the assumed wind statistics. The resulting model is then compared with the JASIN model and with aircraft scatterometer measurements.

2. Wind Vector Probability

SASS sampled the wind vectors over the world's ocean for a 3-month period from July 7 to October 10, 1978. Four dual-polarized (horizontal and vertical) fan beam antennas orientated at 45° angles relative to the subtrack produce an X-shaped illumination pattern on the ocean surface. In this way, the ocean is first viewed by a forward antenna, and then 1 to 3 min later (depending on swath position) is viewed by an aft antenna at an orthogonal direction relative to the forward antenna. Sixty-one 4.8 ms pulses are transmitted to the surface, and the return signals are processed by 15 Doppler filters to obtain individual footprints along the fan beam. These footprints are about 50 km along the fan beam and 17 km across. Three footprints are close to nadir, having incidence angles of approximately 0°, 4°, and 8°. The remaining 12 footprints fall within the incidence angle range from 22° to 65°. The Doppler filtering technique is distorted by the earth's rotation, and as a result the swath width and incidence angle range varies over an orbit. A complete description of the instrument and footprint geometry is given by Bracalente et al. [1980].

During the 3-month life of SASS, 2.7 million h-pol and 19.1 million v-pol measurements of the ocean surface were taken. In our data processing, we stratify these data into 4° incidence angle bins. Each bin contains between 100,000 and 300,000 measurements for h-pol and between 1 and 2 million measurements for v-pol. We let $\{\vec{W}\}$ denote the ensemble of wind vectors $\vec{W}$ that are sampled by a given polarization and incidence angle bin over the entire globe for the 3-month period. We assume $\{\vec{W}\}$ is distributed according to a bivariate normal probability function

$$P(W_x,W_y) = \exp[-(W_x^2 + W_y^2)/2\Delta W^2]/(2\pi\Delta W^2) \qquad (1)$$

where W_x and W_y are two orthogonal components of $\vec{W}$ (for example, along and perpendicular to the antenna beam) and ΔW is the standard deviation of W_x and W_y.

The degree to which $P(W_x,W_y)$ actually represents the frequency distribution of $\{\vec{W}\}$ impacts all subsequent analysis. The assumption that W_x and W_y have a zero mean requires that there is a high degree of variability in the wind vector relative to the antenna observation direction. The cyclonic wind patterns in the mid-latitudes, the easterly trade winds in the tropics, and the westerlies in the poleward latitudes certainly provide this variability, along with the fact that the antenna directions rotate $\pm 72°$ during an orbit. In addition, the results in section 4 show that the average radar returns for the four antennas are nearly equal, indicating that W_x and W_y are indeed zero-mean deviates. Other researchers [Brooks et al., 1946; Davenport, 1967] have also concluded that (1) is an accurate statistical description for the wind vector.

For our purposes, it is more convenient to express $P(W_x,W_y)$ in terms of the wind magnitude W and its direction χ relative to the antenna. Doing this transformation gives

$$P(W,\chi) = W \exp(-W^2/2\Delta W^2)/(2\pi\Delta W^2) \qquad (2)$$

Apart from the factor of $1/2\pi$, this is a Rayleigh distribution in wind speed. The $1/2\pi$ represents a uniform distribution in χ over the range 0 to 2π. The mean wind speed $\bar{W}$ for the distribution is related to ΔW by

$$\bar{W} = (\pi/2)^{\frac{1}{2}}\,\Delta W \qquad (3)$$

Hence, the distribution has only one degree of freedom, the mean wind $\bar{W}$. The U.S. Navy Marine Climatic Atlas [U. S. Navy, 1981] is used to specify $\bar{W}$. For the months of July, August, and September, the mean global climatic wind speed is

7.4 m/s. The SASS v-pol measurements are evenly distributed over the world's oceans for these 3 months, and hence we set $\bar{W}$ = 7.4 m/s for v-pol. However, the h-pol measurements are not uniformly distributed, with a disproportionate number of measurements being at the extreme northern and southern latitudes.

In order to determine $\bar{W}$ for h-pol, we use the SASS I geophysical model [Jones et al., 1982] to compute a mean global wind speed from h-pol and v-pol measurements, separately. The computed h-pol mean wind is 1.1 m/s higher than the v-pol wind. This difference consists of two components: an instrument/model bias and an actual offset due to h-pol heavily sampling the extreme latitudes. The instrument/model bias is found by looking at those time periods for which h-pol and v-pol measurements were taken simultaneously (i.e., SASS modes 3 and 4). For these cases, both polarizations are seeing the same wind fields, and any offset in the retrieved wind must be due to instrument and/or geophysical model biases. For the combined h-pol/v-pol cases, the h-pol wind is 0.5 m/s higher than the v-pol wind. Thus we attribute 0.5 m/s of the total 1.1 m/s offset to instrument/model bias and the remaining 0.6 m/s to the differences in sampling. On the basis of this analysis, the mean wind speed $\bar{W}$ for h-pol is set to 8.0 m/s.

The specification of $\bar{W}$ is, of course, subject to error, although we expect the error to be less than 0.5 m/s. Fortunately, as section 4 shows, the calculation of the NRCS wind sensitivity coefficient α_0 does not depend on $\bar{W}$. The NRCS proportionality coefficient a_0 does depend on $\bar{W}$. This dependence is $(1/\bar{W})^{\alpha_0}$, where α_0 is about 2. Thus, an error in $\bar{W}$ produces a simple multiplicative bias in the NRCS model.

3. NRCS Model Function

Guinard et al. [1971] suggested a simple empirical relationship between the NRCS and wind speed:

$$\sigma^0 = aW^{\alpha} \tag{4}$$

where a and α depend on polarization and incidence angle θ_i. Later experiments by Jones and Schroeder [1978] showed that a and α also depend on the relative azimuth angle χ, which is the observation azimuth direction relative to the wind direction. This χ dependence is such that

$$a = a_0 q \tag{5}$$

$$\alpha = \alpha_0 + \delta \tag{6}$$

where a_0 and α_0 are the average values of a and α over all wind directions. The terms q and δ contain the χ dependence. The term q varies by ± 0.5, or less, about unity, and δ varies by ± 0.2, or less, about zero. Since δ is small compared to unity, one can approximate (4) by

$$\sigma^0 = a_0 q W^{\alpha_0 + \delta}$$

$$\sim a_0 W^{\alpha_0}[q + 2.3q\delta \log W] \tag{7}$$

where 2.3 is the natural logarithm of 10. Note that the approximation in (7) does not necessarily decrease the accuracy of the σ^0 model, since the original expression (4) is only an empirical approximation.

The wind direction terms q and $q\delta$ can be expressed in terms of a partial Fourier series.

$$q = 1 + a_1 \cos \chi + a_2 \cos 2\chi \tag{8}$$

$$2.3q\delta = \alpha_1 \cos \chi + \alpha_2 \cos 2\chi \tag{9}$$

where $q\delta$ varies about zero and hence has no bias term. Since the χ dependence is different for different polarizations and incidence angles, the a's and α's depend on polarization and θ_i. Implicit in (8) and (9) is the assumption that σ^0 is symmetric about the wind direction, and hence there are no sine terms. We only retain the first two harmonics because aircraft experiments conducted by NASA Langley Research Center under the AAFE RADSCAT Program indicate the higher-order harmonics are insignificant (see section 5). Combining (7), (8), and (9) yields

$$\sigma^0 = A_0 + A_1 \cos \chi + A_2 \cos 2\chi \tag{10}$$

$$A_0 = a_0 W^{\alpha_0} \tag{11}$$

$$A_1 = (a_1 + \alpha_1 \log W)A_0 \tag{12}$$

$$A_2 = (a_2 + \alpha_2 \log W)A_0 \tag{13}$$

These four equations define the NRCS model function.

The obvious question is to what degree is the NRCS model given by (10) through (13) an oversimplification. First, it is doubtful that σ^0 increases exactly as a constant power of wind speed, as (11) dictates. However, systematic departures from a power law relationship have yet to be observed and await further investigation. In addition there are a number of other factors that may degrade the accuracy of the NRCS model. The particular nature of the wind turbulence within a footprint, the wind fetch and duration, and the underlying long gravity waves can cause different roughness patterns for the same mean wind vector. Also, Kinsman [1965] pointed out that viscosity is an important parameter in determining the decay time for the shorter capillary waves (~2 cm) that are responsible for Bragg backscattering. Since the viscosity of water increases by a factor of 1.5 as the sea-surface temperature decreases from 30° C to 12° C, the NRCS may also be affected by variations in the sea temperature. However, these secondary dependencies appear to be small, and we do not attempt to model them at this time.

The special case of backscattering for incidence angles near nadir (0° to 8°) is discussed in section 6. For these incidence angles, we assume no wind direction dependence, and the NRCS model is simply given by (11).

4. Determination of Model Parameters

The parameters in the NRCS model function that need to be specified are a_0, a_1, a_2, α_0, α_1, and α_2. Each of these parameters depends on polarization and incidence angle. The parameters pertaining to the zeroth and second harmonics (subscripts 0 and 2) can be found directly from the

statistics of the SASS NRCS measurements. However, we see no direct way to find a_1 and α_1 for the first harmonic from the SASS data. The first harmonic is a measure of the variation of the NRCS over a 180° change in χ. This type of variation was never measured by SASS because a given ocean area was viewed at azimuth angles separated by 90°, not 180°. As discussed in section 5, we rely on AAFE RADSCAT aircraft circle measurements to specify a_1 and α_1.

The NRCS measurements from the forward and aft antennas are first collocated into 50 km square cells. For a given cell, all forward antenna measurements are averaged to obtain $\tilde{\sigma}_1^0$, and all aft measurements are averaged to obtain $\tilde{\sigma}_2^0$.

$$\tilde{\sigma}_1^0 = \sigma_1^0 + \varepsilon_1 \tag{14}$$

$$\tilde{\sigma}_2^0 = \sigma_2^0 + \varepsilon_2 \tag{15}$$

where σ_1^0 and σ_2^0 are the actual NRCS values for the bin and ε_1 and ε_2 are errors due to Rayleigh fading and instrument noise. On the basis of strength of the return power, the SASS sensor algorithm estimates the mean squared errors ε_1^2 and ε_2^2. Note that the mean error is zero. For each cell, the following sum and difference are found:

$$\tilde{s} = (\tilde{\sigma}_1^0 + \tilde{\sigma}_2^0)/2 \tag{16}$$

$$\tilde{d} = (\tilde{\sigma}_1^0 - \tilde{\sigma}_2^0)/2 \tag{17}$$

The mean incidence angle θ_i for the cell is also computed.

The quantities $\tilde{s}$, $\tilde{d}$, ε_1^2, ε_2^2, and θ_i are binned according to polarization and θ_i. The width of the bins is 4°, except for the nadir bin that contains measurements between 0° and 2°. For example, the nth bin corresponds to $\theta_i = 4n \pm 2$, where n=0 to 17. For each polarization and θ_i bin, the following averages are computed over the entire 3 months of SASS ocean measurements:

$$\langle\tilde{s}\rangle_{\theta,\chi,W},\ \langle\tilde{s}^2\rangle_{\theta,\chi,W},\ \langle\tilde{d}\rangle_{\theta,\chi,W},\ \langle\tilde{d}^2\rangle_{\theta,\chi,W},$$

$$\langle(\varepsilon_1^2 + \varepsilon_2^2)/4\rangle_{\theta,\chi,W},\ \langle\theta_i\rangle_{\theta,\chi,W}$$

where $\langle\cdots\rangle_{\theta,\chi,W}$ denotes that the average is over an ensemble of incidence angles ($\pm 2°$ within the bin), wind directions, and wind speeds. There is a noise component in $\langle\tilde{s}^2\rangle_{\theta,\chi,W}$ and $\langle\tilde{d}^2\rangle_{\theta,\chi,W}$ due to ε_1^2 and ε_2^2. This noise component does not occur in the averages $\langle\tilde{s}\rangle_{\theta,\chi,W}$ and $\langle\tilde{d}\rangle_{\theta,\chi,W}$ because the average value of ε_1 and ε_2 is zero. The noise-free values for the averages are

$$\langle s\rangle_{\theta,\chi,W} = \langle\tilde{s}\rangle_{\theta,\chi,W} \tag{18}$$

$$\langle d\rangle_{\theta,\chi,W} = \langle\tilde{d}\rangle_{\theta,\chi,W} \tag{19}$$

$$\langle s^2\rangle_{\theta,\chi,W} = \langle\tilde{s}^2\rangle_{\theta,\chi,W} - \langle(\varepsilon_1^2 + \varepsilon_2^2)/4\rangle_{\theta,\chi,W} \tag{20}$$

$$\langle d^2\rangle_{\theta,\chi,W} = \langle\tilde{d}^2\rangle_{\theta,\chi,W} - \langle(\varepsilon_1^2 + \varepsilon_2^2)/4\rangle_{\theta,\chi,W} \tag{21}$$

The average $\langle d\rangle_{\theta,\chi,W}$ is always very close to zero and is not actually used in the derivation of the model function. For example, the ratio of $\langle d\rangle_{\theta,\chi,W}/\langle s\rangle_{\theta,\chi,W}$ varies from −0.06 to 0.03, depending on θ_i bin and polarization. Thus the average difference between the forward and aft antenna is only a few percent of the average NRCS for both antennas. Our assumption of a uniform distribution for wind direction requires that $\langle d\rangle_{\theta,\chi,W}$ be zero, and the observations are consistent with this assumption. In other words, the forward and aft antennas observed nearly the same NRCS when averaged over 3 months. The small residual values for $\langle d\rangle_{\theta,\chi,W}$ are due to small relative antenna gain biases in the sensor algorithm and/or a slight departure from a uniform wind direction distribution.

We make a small correction for the effect of averaging over a 4° incidence angle bin. Section 7 shows that

$$\langle y\rangle_{\chi,W} = t\langle y\rangle_{\theta,\chi,W} \tag{22}$$

where y denotes either s, s^2, or d^2 and $\langle\cdots\rangle_{\chi,W}$ is an average over χ and W that has been normalized to the mean incidence angle $\langle\theta_i\rangle_{\theta,\chi,W}$ for the bin in question. The parameter t accounts for the fact that the average of y over the incidence angle bin does not necessarily equal the value of y at the average incidence angle for the bin. If y varied linearly with θ_i then the equality would hold, and t would equal 1. However, y actually varies more like $\exp(c\theta_i)$, and as a result t is between 0.93 and 1.

Working with the θ_i corrected averages, one may write

$$\langle s\rangle_{\chi,W} = \int_0^\infty dW \int_0^{2\pi} d\chi\ P(W,\chi)(\sigma_1^0 + \sigma_2^0)/2 \tag{23}$$

$$\langle s^2\rangle_{\chi,W} = \int_0^\infty dW \int_0^{2\pi} d\chi\ P(W,\chi)(\sigma_1^0 + \sigma_2^0)^2/4 \tag{24}$$

$$\langle d^2\rangle_{\chi,W} = \int_0^\infty dW \int_0^{2\pi} d\chi\ P(W,\chi)(\sigma_1^0 - \sigma_2^0)^2/4 \tag{25}$$

where σ_1^0 and σ_2^0 are given by the model function (10). The relative azimuth angles for σ_1^0 and σ_2^0 are denoted by χ_1 and χ_2, where

$$\chi_2 = \chi_1 + \pi/2 \tag{26}$$

The χ integrations are easily done, giving

$$\langle s\rangle_{\chi,W} = \int_0^\infty dW\ P(W)A_0 \tag{27}$$

$$\langle s^2\rangle_{\chi,W} = \int_0^\infty dW\ P(W)(A_0^2 + A_1^2/4) \tag{28}$$

$$\langle d^2\rangle_{\chi,W} = \int_0^\infty dW\ P(W)(A_2^2/2 + A_1^2/4) \tag{29}$$

where P(W) is a Rayleigh distribution in wind speed.

$$P(W) = W \exp(-W^2/2\Delta W^2)/\Delta W^2 \quad (30)$$

As we will show, the value of $A_1^2/4$ is small compared to A_0^2. This fact allows for an iterative solution for a_0 and α_0. To begin, we set A_1 to zero and compute the following ratio

$$\langle s^2\rangle_{\chi,W}/\langle s\rangle^2_{\chi,W} = \frac{\int_0^\infty dW\ P(W)A_0^2}{\left[\int_0^\infty dW\ P(W)A_0\right]^2} \quad (31)$$

Noting that $A_0 = a_0 W^{\alpha_0}$, the integrals can be evaluated in terms of the gamma function. The a_0 coefficients cancel out and one obtains

$$\langle s^2\rangle_{\chi,W}/\langle s\rangle^2_{\chi,W} = \Gamma(1+\alpha_0)/[\Gamma(1+\alpha_0/2)]^2 \quad (32)$$

where $\Gamma(\cdots)$ is the gamma function. Thus under the initial assumption that $A_1 = 0$, the ratio of $\langle s^2\rangle_{\chi,W}$ to $\langle s\rangle^2_{\chi,W}$ depends only on α_0 via the gamma function ratio. It is interesting that the ratio does not even depend on our choice for the mean wind speed $\bar{W}$. As α_0 increases from zero, the gamma function ratio monotonically increases from unity. We compute a table of the gamma function ratio versus α_0 for α_0 increments of 0.01. The table is then used to look up α_0, given $\langle s^2\rangle_{\chi,W}/\langle s\rangle^2_{\chi,W}$. Having found α_0, we next compute a_0 by inverting (27).

$$a_0 = \langle s\rangle_{\chi,W}/[(2\Delta W^2)^{\alpha_0/2}\ \Gamma(1+\alpha_0/2)] \quad (33)$$

In the second iteration, A_1 is not set to zero but rather is given by

$$A_1 = (a_1 + \alpha_1 \log W)a_0 W^{\alpha_0} \quad (34)$$

which corresponds to (12). The parameters a_0 and α_0 come from the first iteration, and a_1 and α_1 are derived from aircraft data. The A_1 component of $\langle s^2\rangle_{\chi,W}$ is then subtracted out. That is to say, in (31) and (32) the term $\langle s^2\rangle_{\chi,W}$ is replaced by

$$\langle s^2\rangle'_{\chi,W} = \langle s^2\rangle_{\chi,W} - \int_0^\infty dW\ P(W)A_1^2/4 \quad (35)$$

where the integral is numerically evaluated using $dW = 0.1$ m/s. Having corrected for the A_1 term, we then find α_0 and a_0 in the same way as in the first iteration. The A_1 term is small compared to the A_0 term, and the new α_0 changes by 2% or less from those found in the first iteration. Only two iterations are required for adequate convergence.

The two remaining parameters to be found are a_1 and α_1. In order to find these two parameters, we must further stratify the measurements in a given bin according to the mean NRCS value $\tilde{s}$. To be specific, an observation is put into one of five different levels:

level 1: $\tilde{s}/\langle\tilde{s}\rangle_{\theta,\chi,W}$ less than −4.5 dB,
level 2: $\tilde{s}/\langle\tilde{s}\rangle_{\theta,\chi,W}$ between −4.5 and −1.5 dB,
level 3: $\tilde{s}/\langle\tilde{s}\rangle_{\theta,\chi,W}$ between −1.5 and 1.5 dB,
level 4: $\tilde{s}/\langle\tilde{s}\rangle_{\theta,\chi,W}$ between 1.5 and 4.5 dB,
level 5: $\tilde{s}/\langle\tilde{s}\rangle_{\theta,\chi,W}$ greater than 4.5 dB,

where $\langle\tilde{s}\rangle_{\theta,\chi,W}$ is the average of all the $\tilde{s}$ values contained in the polarization and incidence angle bin under consideration. Then in a manner analagous to that discussed above, the data in each level are averaged over the 3 months of SASS ocean measurements, the noise component is subtracted out, and the incidence angle correction is made. The result of this data processing is two averages of the form

$$\langle s^2\rangle_{\chi,W,j} = \int_{W_j}^{W_{j+1}} dW\ P(W)(A_0^2 + A_1^2/4) \quad (36)$$

$$\langle d^2\rangle_{\chi,W,j} = \int_{W_j}^{W_{j+1}} dW\ P(W)(A_2^2/2 + A_1^2/4) \quad (37)$$

where the subscript j indicates the average is for the jth level. The term W_j corresponds to the lower wind speed limit for the jth level. It is calculated from the lowest mean NRCS measurement $\tilde{s}_j$ in the j level. According to the model function (10) and definition (16), $\tilde{s}_j$ is given by

$$\tilde{s}_j = A_0 + A_1[\cos\chi_1 - \sin\chi_1]/2 + (\varepsilon_1+\varepsilon_2)/2 \quad (38)$$

Neglecting the noise term and the A_1 term, which is small compared to the A_0 term, and using (11), one obtains a good approximation for the wind speed that would produce the observation $\tilde{s}_j$

$$W_j = (\tilde{s}_j/a_0)^{1/\alpha_0} \quad (39)$$

where a_0 and α_0 have been derived above. The value of $\tilde{s}_j$ for level 1 is zero, giving $W_1 = 0$. For levels 2 to 5, $\tilde{s}_j$ is given by

$$\tilde{s}_j = 10^n\langle\tilde{s}\rangle_{\theta,\chi,W} \quad (40)$$

where $n = -0.45$, -0.15, 0.15, and 0.45 for $j = 2$ to 5, respectively. The value of W_6, which is the upper wind speed limit for level 5, is set to infinity.

Having determined the wind speed ranges for each level, we then find a_2 and α_2. This is done by first computing the following:

$$Y_j^2 = \frac{2\langle d^2\rangle_{\chi,W,j} - \int_{W_j}^{W_{j+1}} dW\ P(W)A_1^2/2}{\langle s^2\rangle_{\chi,W,j} - \int_{W_j}^{W_{j+1}} dW\ P(W)A_1^2/4} \quad (41)$$

where there is now sufficient information to numerically compute the two integrals. In terms

of a_2 and α_2, the quantity Y_j is given by

$$Y_j^2 = \frac{\int_{W_j}^{W_{j+1}} dW\, P(W)(a_2 + \alpha_2 \log W)^2 A_0^2}{\int_{W_j}^{W_{j+1}} dW\, P(W) A_0^2} \qquad (42)$$

In the above expression, the log W term varies slowly compared to the A_0 term, and there exists an effective wind speed $\bar{W}_j$ for which

$$Y_j = a_2 + \alpha_2 \log \bar{W}_j \qquad (43)$$

where $\bar{W}_j$ is close to the mean wind speed for the j level. Numerical simulations show that $\log \bar{W}_j$ is accurately approximated by

$$(\log \bar{W}_j)^2 = \frac{\int_{W_j}^{W_{j+1}} dW\, P(W)(A_0 \log W)^2}{\int_{W_j}^{W_{j+1}} dW\, P(W) A_0^2} \qquad (44)$$

In terms of Y_j, the error introduced by this approximation is 0.5% or less. Using (41) and (44), five values for Y_j and $\log \bar{W}_j$ are computed for the five levels. A least-squares fit to the five points is then done to determine a_2 and α_2 according to (43).

For incidence angles greater than 52°, the 50 km cells do not contain NRCS measurements from both the forward and aft antennas, and the above derivation cannot be used. However, it is possible to obtain a value for the coefficient A_0. For incidence angles bins above 52°, the NRCS measurements are simply averaged together without regard to antenna. At certain times in the orbit the forward antenna footprints will extend out to these high incidence angles, and at other times the aft antenna will. Averaged over an orbit, there will be approximately the same number of forward and aft measurements in a given incidence angle bin. This type of average has the same statistical properties as $\langle s \rangle_{\chi,W}$, and as such can be used in (33) to compute a_0, given α_0. For α_0, we used the value found at 52°. The computed a_0 and assumed α_0 are then used to calculate the value of A_0 at 10 m/s, which is given by

$$A_0 = a_0 10^{\alpha_0} \qquad (45)$$

Fortunately, the value of A_0 at 10 m/s is insensitive to the choice of α_0. A positive error in α_0 will cause a_0 to decrease and 10^{α_0} to increase. The resulting error in A_0 is small, being about 5% for an estimated 0.2 error in α_0.

5. Analysis of Aircraft Data

During the 1970's, NASA Langley Research Center flew a series of aircraft scatterometer missions under the AAFE RADSCAT Program [Jones and Schroeder, 1978]. In our analysis, the aircraft measurements from missions 238, 306, 318, and 335 are used to determine the NRCS model parameters a_1, α_1, a_2, and α_2. We do not attempt to determine a_0 and α_0 because they are sensitive to biases in the aircraft data and errors in the in situ data. During these missions, the aircraft flew circles such that the relative azimuth angle χ varies from 0° to 360°. The NRCS measurements were integrated and dumped every 10°. The incidence angle θ_i stayed relatively constant during a circle, and a correction is made to account for any small θ_i variations. Throughout the circles, the polarization was continuously switched between horizontal and vertical.

A harmonic analysis is done on the 36 measurements in each circle. The amplitude of the first four sine and cosine harmonics, χ to 4χ, along with the bias term are found. The results indicate that the only statistically significant terms are the bias, cos χ, and cos 2χ. That is to say, the aircraft circle data are well represented by (10). According to (12) and (13) one has

$$A_1/A_0 = a_1 + \alpha_1 \log W \qquad (46)$$

$$A_2/A_0 = a_2 + \alpha_2 \log W \qquad (47)$$

where in this case A_0, A_1, and A_2 come from the harmonic analysis of the aircraft circle data. For each polarization, the circle data are placed into one of four incidence angle groupings. The ranges of θ_i for the four groups are 19° - 20°, 28° - 31°, 39° - 40°, and 48° - 65°. The number of circles for each group is 10, 7, 10, and 13, respectively, and each circle is for a different wind speed. The wind speeds range from 4 to 25 m/s. Least-squares fits of A_1/A_0 and A_2/A_0 versus log W provide values for a_1, α_1, a_2, and α_2 for each θ_i group and polarization. Fortunately, any multiplicative biases that may be present in the aircraft measurements cancel when calculating the ratios A_1/A_0 and A_2/A_0. The values of a_1, α_1, a_2, and α_2 determined from the aircraft data are presented in Section 9.

In section 4, the derivation of the model parameters from SASS data requires that a_1 and α_1 be specified for each of the 4° incidence angle bins. The aircraft results suggest that the following linear relationship exists between a_1, α_1, and θ_i

$$a_1 = b(\theta_i - 20) \qquad 20° \geq \theta_i \geq 56° \qquad (48)$$

$$\alpha_1 = \beta(\theta_i - 20) \qquad 20° \geq \theta_i > 56° \qquad (49)$$

The value of b is 0.0289 and 0.0086 for h-pol and v-pol, respectively. The value of β is -0.0162 and -0.0040 for h-pol and v-pol, respectively. Thus h-pol has a much larger first harmonic than v-pol. For $\theta_i < 20°$, a_1 and α_1 are assumed to be zero. This assumption is based on the fact that a_1 and α_1 must be zero at $\theta_i = 0$ and that they are near zero for the 20° aircraft data. The parameters a_1 and α_1 need only be specified to 52° because the binned SASS data only extend to 52°.

6. Nadir Model Function

The derivation of the model function for incidence angles near nadir (0° to 8°) is nearly the same as that described in section 4, with one major exception. The NRCS measurements near 0° that fall in level 5 (i.e., $\tilde{s}/\langle\tilde{s}\rangle_{\theta,\chi,W} > 4.5$ dB) display a very large variation. Level 5 contains the largest NRCS values, and for nadir backscattering this corresponds to specular reflections from a calm sea surface. These specular returns show up as spikes that are 10 to 20 dB higher than the NRCS for moderate winds. These spikes distort the statistical quantities $\langle s\rangle_{\chi,W}$, $\langle s^2\rangle_{\chi,W}$, and $\langle d^2\rangle_{\chi,W}$. In view of this, we eliminated all level 5 measurements from our derivation of the nadir model function.

The near-nadir observations show little, if any, dependence on wind direction. For example, $\langle d^2\rangle^{\frac{1}{2}}_{\chi,W}/\langle s\rangle_{\chi,W}$, which is a good indication of wind direction dependence, is about 0.07 for the near-nadir observations as compared with 0.30 to 0.50 for the off-nadir observations. As discussed in section 8, this small 0.07 variation is probably due to wind gradients in the 50 km cells, rather than wind direction effects. Thus we assume A_1 and A_2 are zero for near nadir (they must be zero at nadir), and the only parameters we need to find are a_0 and α_0.

The exclusion of the low wind speed measurements alters the lower limit of the integrals in equation (31) that is used to determine α_0. For the nadir analysis, (31) becomes

$$\langle s^2\rangle_{\chi,W}/\langle s\rangle^2_{\chi,W} = \frac{\int_{W_1}^{\infty} dW\ P(W)A_0^2}{\left[\int_{W_1}^{\infty} dW\ P(W)A_0\right]^2} \tag{50}$$

The lower wind speed limit W_1 is determined from the fraction of observations that occur in level 5. For example, the v-pol, nadir bin ($0° \le \theta_i \le 2°$) contains 248943 observations. Of this total, 5377 observations fall in level 5. Thus level 5 contains 2.16% of the observations. In terms of the wind speed probability P(W) this fraction F of level 5 observations is given by

$$F = \int_0^{W_1} dW\ P(W) \tag{51}$$

where in this case F = 0.0216. We generate a table of F versus W_1 from which W_1 can be looked up given F. For h-pol, the values of W_1 are 1.4, 0.8, and 0 m/s for the 0°, 4°, and 8° incidence angle bins, respectively. For v-pol, the W_1 values are 1.2, 0.9, and 0 m/s. At 8°, no observations fall in level 5 and hence $W_1 = 0$.

Once W_1 is known, the integrals in (50) are numerically evaluated as a function of α_0. Geometric optics predicts at 0° the NRCS decreases monotonically as W increases, and hence α_0 is negative. At 4° (8°) geometric optics predicts that the NRCS increases as the wind speed goes from 0 to about 1 m/s (5 m/s), at which point it reaches a maximum, and then begins to decrease at higher wind speeds. Since most of the SASS observations are for winds above 1 m/s (5 m/s), we assume α_0 is also negative at 4° (8°). However, this dependence of the 4° and 8° NRCS on wind speed is clearly not in agreement with the power law relationship given by (11), and our results must be viewed with caution at these angles. For negative α_0, the ratio of integrals in (50) monotonically increases from unity as α_0 decreases from zero. Accordingly, the value α_0 is incremented by −0.01 from zero until the equality specified by (50) is satisfied. Having found α_0, we compute a_1 from

$$a_0 = \langle s\rangle_{\chi,W} \Big/ \int_{W_1}^{\infty} dW\ P(W)W^{\alpha_0} \tag{52}$$

which is a modified version of (33) to account for the exclusion of level 5 data.

7. Incidence Angle Correction

A small correction is made to account for the nonlinear relationship between $\langle y\rangle_{\theta,\chi,W}$ and θ_i, where y denotes s, s^2, or d^2. The plots of $\ln\langle y\rangle_{\theta,\chi,W}$ versus θ_i are much more linear than plots of $\langle y\rangle_{\theta,\chi,W}$ versus θ_i. An analysis of these plots indicate that within a 4° bin, the incidence angle variation of the χ,W average is well approximated by

$$\langle y(\theta_i)\rangle_{\chi,W} = \langle y\rangle_{\chi,W} \exp[c(\theta_i - \bar{\theta}_i)] \tag{53}$$

where $\langle y\rangle_{\chi,W}$ is the value of the χ,W average at the mean incidence angle $\bar{\theta}_i$ for the bin ($\bar{\theta}_i = \langle\theta_i\rangle_{\theta,\chi,W}$). The parameter c is the slope of the $\ln\langle y\rangle_{\theta,\chi,W}$ versus θ_i plots. The measurements are evenly distributed within a bin, and one may write

$$\langle y\rangle_{\theta,\chi,W} = \int_{\theta_1}^{\theta_2} d\theta_i\ \langle y\rangle_{\chi,W} \exp[c(\theta_i - \bar{\theta}_i)]/(\theta_2 - \theta_1) \tag{54}$$

where θ_1 and θ_2 are the lower and upper θ_i limits for the bin. The assumption of even distribution requires

$$\bar{\theta}_i = (\theta_2 + \theta_1)/2 \tag{55}$$

Solving the integral using (55) gives

$$\langle y\rangle_{\theta,\chi,W} = \langle y\rangle_{\chi,W} \sinh z/z \tag{56}$$

$$z = c(\theta_2 - \theta_1)/2 \tag{57}$$

Thus the incidence angle correction consists of dividing the ensemble average $\langle y\rangle_{\theta,\chi,W}$ by $\sinh z/z$. The result is the ensemble average $\langle y\rangle_{\chi,W}$ at the mean incidence angle $\bar{\theta}_i$. In all cases, this correction is small, with $\sinh z/z$ being between 1 and 1.08.

8. Errors Due to Wind Gradient, Incidence Angle, and Aircraft Data

The footprints from the forward and aft antennas do not exactly coincide. We only require that both footprint centroids lie in the same 50 km square cell. A worst case would have the centroids at opposite corners separated by 71 km, but on the average the separation is only 30 km. Even when the centroids coincide, the footprint areas, which are about 17 by 50 km rectangles, will cover different portions of the ocean because the rectangles are orthogonal. Hence in the presence of wind gradients, the average wind vector over one footprint is different from that over the other. The major impact of this wind gradient effect is that it will add a bias to the statistical quantity $\langle d^2 \rangle_{\chi,W}$. The other quantities $\langle s \rangle_{\chi,W}$, $\langle s^2 \rangle_{\chi,W}$, and $\langle d \rangle_{\chi,W}$ are insensitive to the gradient effect. To be specific, one may write

$$\langle d^2 \rangle_{\chi,W} = V_\chi + V_g \tag{58}$$

where V_χ is the variance due to the 90° relative wind direction difference between the forward and aft footprints and V_g is the variance due to the wind gradient. The variance V_χ is the desired quantity, and V_g is an unwanted bias. To estimate the magnitude of V_g, we assume the wind speed difference between the forward and aft footprints has a zero mean and a standard deviation of 0.5 m/s. A change in wind speed of 0.5 m/s over an average separation distance of 30 km is probably typical for many ocean scenes. Simulations are then done to compute V_g. The results show that for the off-nadir bins ($\theta_i \geq 24°$), V_g is much less than the observed $\langle d^2 \rangle_{\chi,W}$, with $V_g/\langle d^2 \rangle_{\chi,W}$ being about 3%. The quantity $\langle d^2 \rangle_{\chi,W}$ is used to determine the parameters a_2 and α_2, which are approximately proportional to the square root of $\langle d^2 \rangle_{\chi,W}$. Because of this square root relationship, the error in a_2 and α_2 due to V_g is only 1.5%. At nadir there is no directional effect, and V_χ is zero. In this case $\langle d^2 \rangle_{\chi,W}$ is a direct measure of V_g. The observed normalized variation in terms of $\langle d^2 \rangle^{\frac{1}{2}}_{\chi,W}/\langle s \rangle_{\chi,W}$ is 0.07, which is the same value given by the simulations assuming a wind gradient of 0.5 m/s per 30 km. Thus the assumed gradient is consistent with the nadir data.

Another possible error source is an incidence angle adjustment between the forward and aft footprints. Earth rotation and the misregistration within the 50 km cell cause the incidence angles for the forward and aft footprints to be different. This difference is on the average between 3° and 4°. In the adjustment, the two NRCS values are slightly modified so that they will correspond to an incidence angle that is the average of the forward and aft θ_i. In doing this, the NRCS having the larger θ_i is increased, and the NRCS having the smaller θ_i is decreased. The SASS I geophysical algorithm [Jones et al., 1982] is used to compute the adjustment. The algorithm computes a wind speed and wind direction from the two NRCS values. The wind speed and direction in conjunction with the SASS I GH Table [Schroeder et al., 1982] are then used to compute the slope of the NRCS versus incidence angle. We estimate that the error in the calculated slope is probably about 20%, due to measurement noise and modeling uncertainties. A 20% error in slope translates into a 2% to 4% error in $\langle d^2 \rangle^{\frac{1}{2}}_{\chi,W}$, and likewise in a_2 and α_2. Fortunately the statistical quantities $\langle s \rangle_{\chi,W}$ and $\langle s^2 \rangle_{\chi,W}$ are insensitive to an error in the θ_i adjustment because when the two NRCS values are summed, the errors in the calculated slope have opposite signs and cancel. As with the wind gradient error discussed above, the θ_i adjustment error will always tend to bias $\langle d^2 \rangle_{\chi,W}$ too high.

A small error in the computation of a_0, α_0, a_2, and α_2 will result from errors in the aircraft-derived coefficient A_1. To estimate this error, we consider the case in which there is no upwind/downwind asymmetry (i.e., $A_1=0$). That is to say, we assume the aircraft A_1 is in error by 100%, which is certainly a worst-case situation. For this case and h-pol, the computed α_0 is only 1% to 2% greater than that obtained using the aircraft value for A_1. For v-pol the error is less than 1%. Thus the sensitivity of α_0 to errors in the aircraft data is negligible. The parameter a_0 is computed from (33), which depends on α_0 but not A_1. As a result, a_0 is also insensitive to errors in A_1. The second harmonic parameters a_2 and α_2 are more sensitive to variations in A_1. The worst case is h-pol at 52°, for which $a_2+\alpha_2$ increases by 16% and α_2 decreases by 0.12 when A_1 is set to zero. At the lower incidence angles for h-pol, these changes are only 2% and 0.02, respectively. For v-pol, the errors are always small, being about 1% and 0.01, respectively. In conclusion, the sensitivity of a_0, α_0, a_2 and α_2 to errors in A_1 is very small, except at large incidence angles for h-pol, where the error in a_2 and α_2 may be significant.

Of the four parameters, α_2 probably has the greatest uncertainty. Its derivation requires stratifying the data into five wind speed levels in order to determine the wind speed variation of A_2/A_0. This additional stratification of the data reduces the number of observations in the averages $\langle s^2 \rangle$ and $\langle d^2 \rangle$, particularly for the levels 1 and 5.

9. Results

In this section we present plots of the NRCS model parameters versus incidence angle. These parameters are compared with those obtained from JASIN [Schroeder et al., 1982] and from the RADSCAT aircraft circle flights. For the purpose of discussion, we will use SASS I to denote the JASIN results and SASS II to denote the results obtained from the statistical analysis described herein. The SASS I parameters are found by harmonically analyzing the GH table that gives the NRCS for incidence angles every 2° and relative azimuth angle χ every 10°. For each incidence angle, a harmonic analysis is done to find A_0, A_1, and A_2 according to (10). These three coefficients are calculated for five wind speeds ranging from 3 to 20 m/s. Regressions of log A_0,

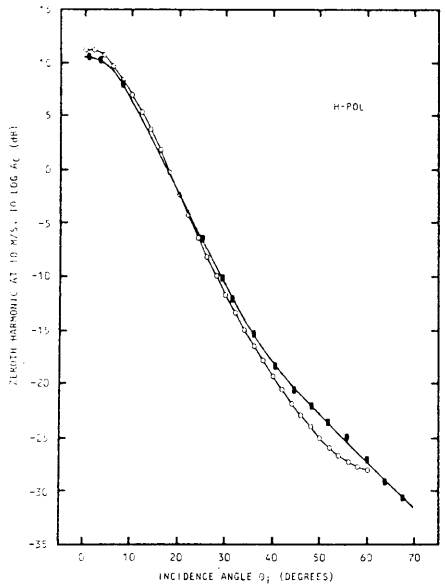

Fig. 2. A comparison of the h-pol NRCS averaged over wind direction at 10 m/s for SASS I (open circles) and SASS II (solid circles).

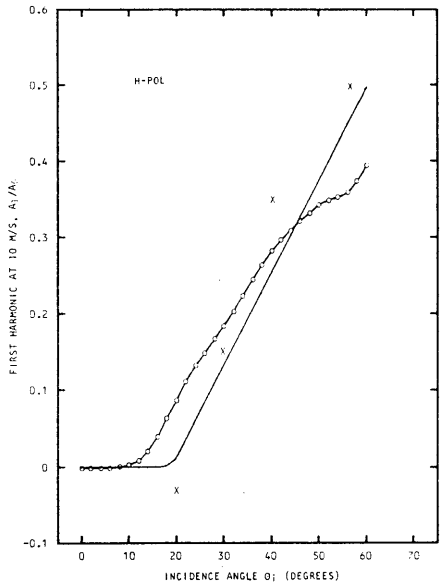

Fig. 4. A comparison of the h-pol NRCS first harmonic at 10 m/s for SASS I (open circles) and aircraft (crosses).

A_1/A_0, and A_2/A_0 versus log W are then performed to determine a_0, a_1, a_2, α_0, α_1, and α_2. We only present SASS I results out to 60°. At higher incidence angles where there are no paired SASS measurements, SASS I is an arbitrary extrapolation having no physical or experimental basis.

Figures 2 and 3 show 10 log A_0, evaluated at 10 m/s, plotted versus incidence angle for horizontal and vertical polarizations, respectively. In terms of the model parameters this quantity equals

$$10 \log A_0 = 10(\alpha_0 + \log a_0) \quad W = 10 \text{ m/s} \qquad (59)$$

and represents the NRCS in decibels averaged over wind direction for a wind speed of 10 m/s. In these and subsequent figures, the solid circles are the SASS II values, and the smaller open circles are the SASS I values. Each solid circle represents a 4° incidence angle bin. The curve drawn through the solid circles is a hand-drawn best fit to the data. For the case of A_0, the incidence angle bins extend out to 68°, as discussed at the end of section 4. For all other parameters the incidence angle bins extend only to 52° because the 50 km cells at higher incidence angles do not contain NRCS measurements from both the forward and aft antenna. The

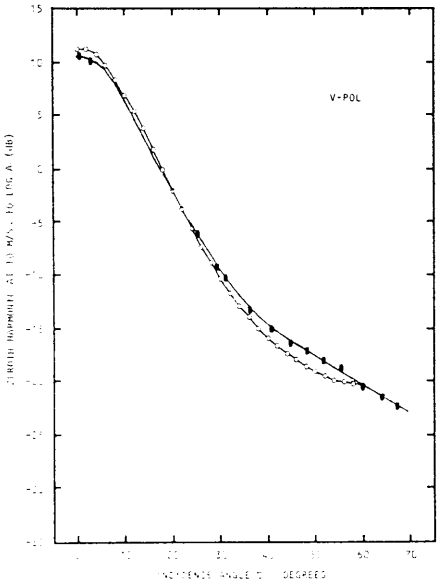

Fig. 3. A comparison of the v-pol NRCS averaged over wind direction at 10 m/s for SASS I (open circles) and SASS II (solid circles).

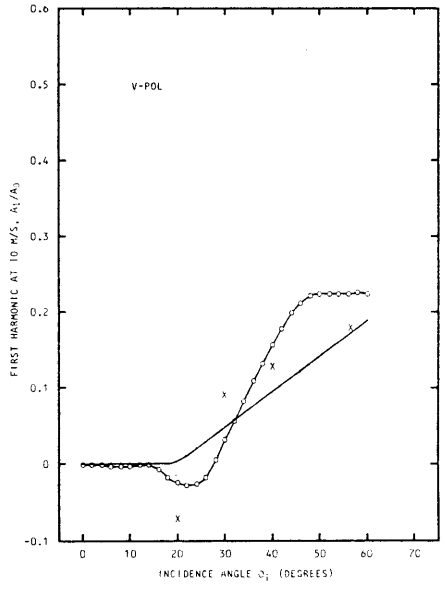

Fig. 5. A comparison of the v-pol NRCS first harmonic at 10 m/s for SASS I (open circles) and aircraft (crosses).

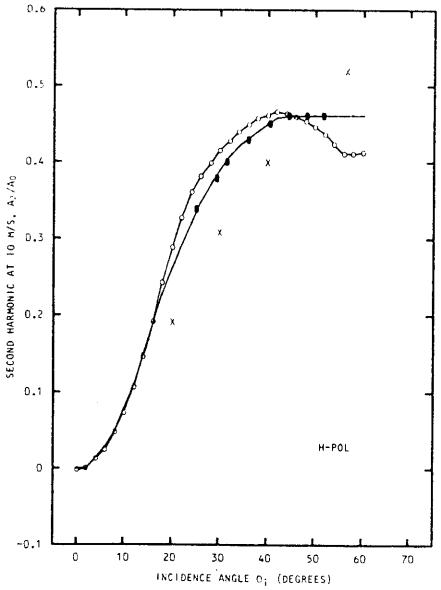

Fig. 6. A comparison of the h-pol NRCS second harmonic at 10 m/s for SASS I (open circles), SASS II (solid circles), and aircraft (crosses).

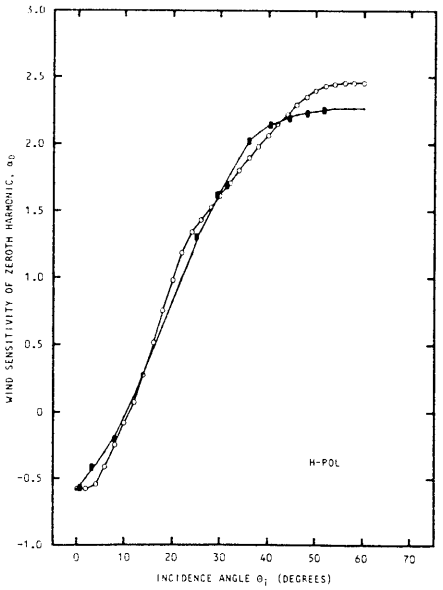

Fig. 8. A comparison of the wind speed sensitivity of the h-pol NRCS averaged over wind direction for SASS I (open circles) and SASS II (solid circles).

SASS I and SASS II values for 10 log A_0 both show the familiar drop off of NRCS with incidence angle. At nadir the SASS II values are about 1 dB lower than SASS I, whereas at the larger incidence angles the SASS II values are higher. The largest discrepancy occurs near 50°, where SASS II is about 2 dB higher.

The next quantity we consider is the ratio A_1/A_0, evaluated at 10 m/s. Figures 4 and 5 show this ratio for horizontal and vertical polarization, respectively. In terms of the NRCS model parameters the ratio is

$$A_1/A_0 = a_1 + \alpha_1 \qquad W = 10 \text{ m/s} \qquad (60)$$

and represents the normalized amplitude of the NRCS first harmonic. As discussed above, we could not obtain this value from the SASS data. Rather, we use the RADSCAT aircraft circle flights. The crosses in Figures 4 and 5 show the aircraft derived values, and the solid line is the fit to these data given by (48) and (49). The agreement between SASS I and aircraft is reasonably good, both showing an increase in A_1/A_0 with incidence angle and considerably larger values for h-pol than for v-pol. The 'bumpy' appearance of the SASS I curves in these and

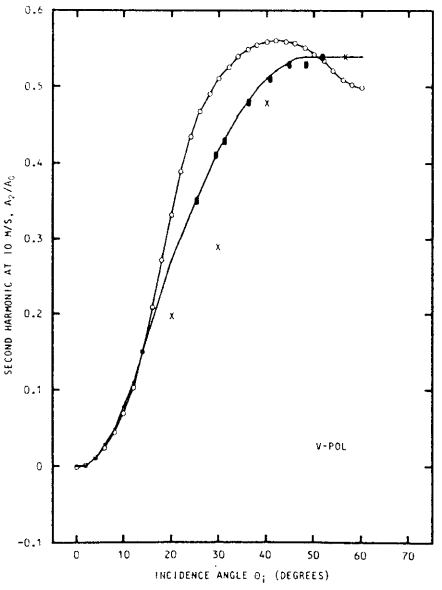

Fig. 7. A comparison of the v-pol NRCS second harmonic at 10 m/s for SASS I (open circles), SASS II (solid circles), and aircraft (crosses).

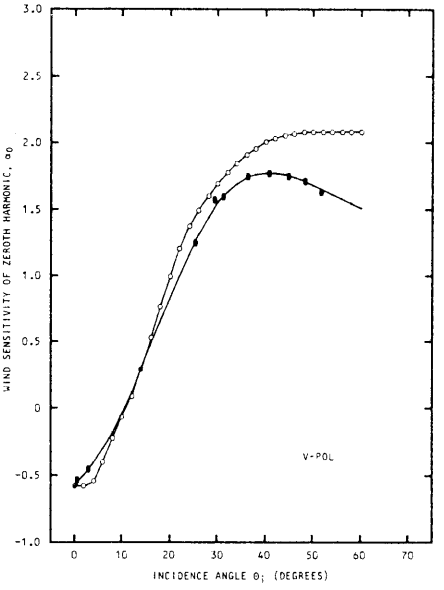

Fig. 9. A comparison of the wind speed sensitivity of the v-pol NRCS averaged over wind direction for SASS I (open circles) and SASS II (solid circles).

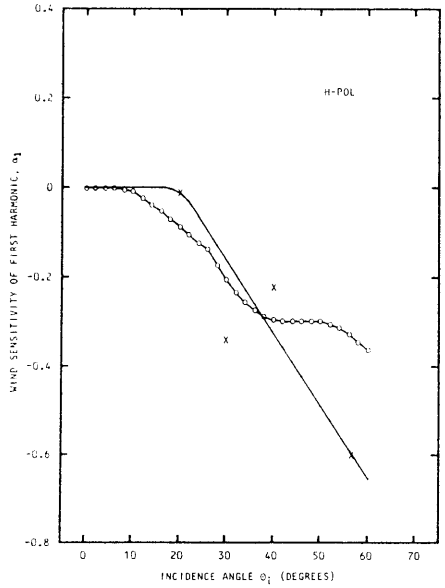

Fig. 10. A comparison of the wind speed sensitivity of the h-pol NRCS first harmonic for SASS I (open circles) and aircraft (crosses).

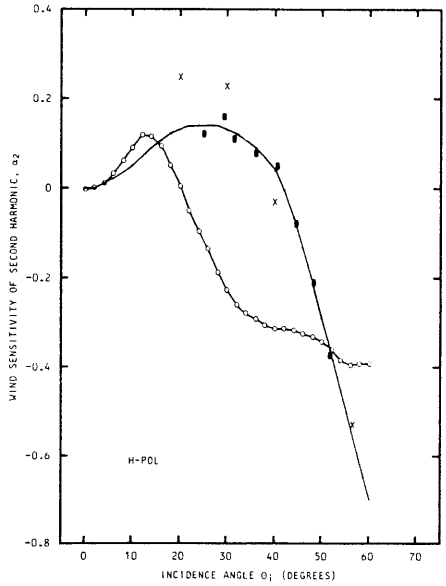

Fig. 12. A comparison of the wind speed sensitivity of the h-pol NRCS second harmonic for SASS I (open circles), SASS II (solid circles), and aircraft (crosses).

subsequent figures is due to the numerous small empirical corrections made to the GH table. As such, these bumps are an artifact of too many degrees of freedom in the model tuning, rather than anything real.

In Figures 6 and 7, the normalized second harmonic A_2/A_0 at 10 m/s is shown for horizontal and vertical polarizations. This ratio is given by

$$A_2/A_0 = a_2 + \alpha_2 \qquad W = 10 \text{ m/s} \qquad (61)$$

In these two figures the SASS I values and SASS II values appear along with the aircraft values denoted by crosses. All three values show the same basic trend of A_2/A_0 increasing with θ_i, with the trend being slightly greater for v-pol. For h-pol there is good agreement between the SASS I and SASS II values, with the aircraft values being somewhat smaller except at 56°. For v-pol the SASS II values lie between the higher SASS I values and the lower aircraft values. Also, the SASS I curve shows a decrease with incidence angle above 40°, whereas the SASS II and aircraft data points seem to flatten out. In

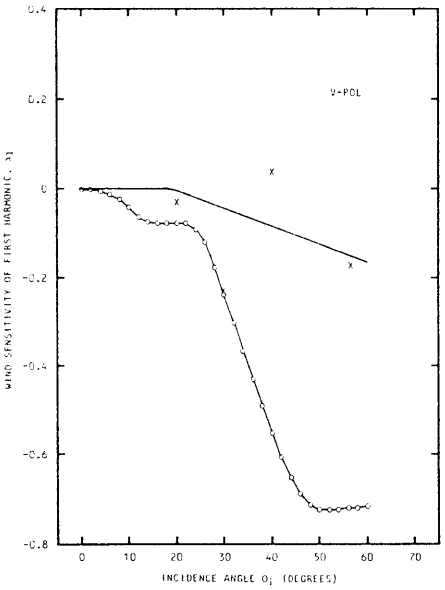

Fig. 11. A comparison of the wind speed sensitivity of the v-pol NRCS first harmonic for SASS I (open circles) and aircraft (crosses).

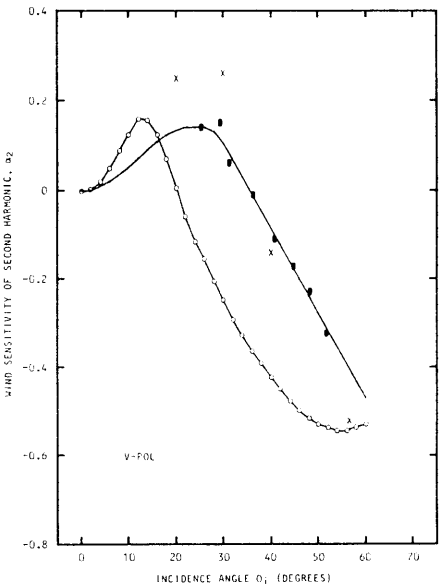

Fig. 13. A comparison of the wind speed sensitivity of the v-pol NRCS second harmonic for SASS I (open circles), SASS II (solid circles), and aircraft (crosses).

TABLE 1. NRCS Model Parameters for Horizontal Polarization

θ_i	$10(\alpha_0+\log a_0)$	$a_1+\alpha_1$	$a_2+\alpha_2$	α_0	α_1	α_2
0	10.5	0.00	0.00	-0.58	0.00	0.00
2	10.4	0.00	0.00	-0.50	0.00	0.00
4	10.0	0.00	0.01	-0.41	0.00	0.01
6	9.2	0.00	0.03	-0.30	0.00	0.02
8	7.9	0.00	0.05	-0.18	0.00	0.03
10	6.3	0.00	0.08	-0.04	0.00	0.05
12	4.6	0.00	0.11	0.12	0.00	0.07
14	2.9	0.00	0.15	0.29	0.00	0.09
16	1.2	0.00	0.19	0.46	0.00	0.11
18	-0.5	0.00	0.23	0.64	0.00	0.12
20	-2.2	0.01	0.26	0.82	-0.01	0.13
22	-3.9	0.03	0.29	1.00	-0.03	0.14
24	-5.6	0.05	0.32	1.17	-0.06	0.14
26	-7.3	0.08	0.35	1.34	-0.10	0.14
28	-9.0	0.10	0.37	1.50	-0.13	0.14
30	-10.7	0.13	0.39	1.64	-0.16	0.13
32	-12.4	0.15	0.41	1.77	-0.19	0.12
34	-14.0	0.18	0.42	1.89	-0.23	0.11
36	-15.4	0.20	0.43	2.00	-0.26	0.09
38	-16.7	0.23	0.44	2.08	-0.29	0.07
40	-17.9	0.25	0.45	2.13	-0.32	0.04
42	-19.1	0.28	0.46	2.16	-0.36	0.00
44	-20.1	0.30	0.46	2.19	-0.39	-0.06
46	-21.0	0.33	0.46	2.21	-0.42	-0.13
48	-21.9	0.36	0.46	2.23	-0.45	-0.21
50	-22.8	0.38	0.46	2.24	-0.49	-0.29
52	-23.7	0.41	0.46	2.25	-0.52	-0.37
54	-24.6	0.43	0.46	2.26	-0.55	-0.45
56	-25.4	0.46	0.46	2.26	-0.58	-0.53
58	-26.3	0.48	0.46	2.26	-0.62	-0.61
60	-27.2	0.51	0.46	2.26	-0.65	-0.69
62	-28.1	—	—	—	—	—
64	-29.0	—	—	—	—	—
66	-29.8	—	—	—	—	—
68	-30.7	—	—	—	—	—
70	-31.6	—	—	—	—	—

drawing the best fit curve to the SASS II data points, we assume that A_2/A_0 is zero at 0° and increases smoothly from 0° to the first actual data point at 24°. As discussed in section 6, the nadir data supports the assumption that A_2/A_0 is zero near 0°, but since there are no data in the region from 8° to 24°, this portion of the curve may be in error.

In the remaining figures, we show the wind speed sensitivity coefficients α_0, α_1, and α_2. Figures 8 and 9 show α_0 plotted versus incidence angle for horizontal and vertical polarization. Both the SASS I and SASS II values show a negative sensitivity at the near-nadir incidence angles (NRCS decreases with wind speed) and a positive sensitivity at the larger incidence angles. At 0° the SASS I and SASS II values are nearly equal, but at 4° a discrepancy exists. It should be noted that when deriving the SASS I GH table little attention was paid to the 4° data. For h-pol there is fair agreement with the two curves interweaving. For v-pol the SASS II values for incidence angles of 24° and greater are substantially less than the SASS I values. Also, the SASS II α_0's reach a maximum near 40° and then decrease, whereas SASS I is flat.

The α_1 values are shown in Figures 10 and 11. As with the coefficient A_1/A_0, there are no SASS II values. The four crosses are the aircraft values, and the solid line is the best fit to the aircraft data given by (49). For h-pol, the agreement between the aircraft and SASS I is fairly good, except at the highest incidence angle of 56°, at which the aircraft α_1 is much larger in a negative sense than the SASS I value. For v-pol the agreement is poor. The SASS I α_1's decrease sharply with incidence angle, whereas the aircraft α_1's depart only slightly from zero. In fact, the SASS I v-pol values are larger in a negative sense than the SASS I h-pol values, which clearly contradicts the aircraft results.

Finally, Figures 12 and 13 show the wind sensitivity α_2 of the second harmonic plotted versus incidence angle for the two polarizations. These figures contain values for SASS I, SASS II, and aircraft. In drawing the curve through the SASS II data points, we require that α_2 is zero at 0° and construct a smooth interpolation to connect 0° with the 24° value. The SASS II and aircraft values are in good agreement except that the aircraft α_2's are somewhat larger between 20° and 30°. The SASS I curves fall considerably below both the aircraft and SASS II results, except at the higher incidence angles.

TABLE 2. NRCS Model Parameters for Vertical Polarization

θ_i	$10(\alpha_0+\log a_0)$	$a_1+\alpha_1$	$a_2+\alpha_2$	α_0	α_1	α_2
0	10.5	0.00	0.00	-0.58	0.00	0.00
2	10.4	0.00	0.00	-0.50	0.00	0.00
4	10.0	0.00	0.01	-0.41	0.00	0.01
6	9.2	0.00	0.03	-0.30	0.00	0.02
8	7.9	0.00	0.05	-0.18	0.00	0.03
10	6.3	0.00	0.08	-0.04	0.00	0.05
12	4.6	0.00	0.11	0.12	0.00	0.07
14	2.9	0.00	0.15	0.29	0.00	0.09
16	1.2	0.00	0.19	0.46	0.00	0.11
18	-0.4	0.00	0.23	0.64	0.00	0.12
20	-2.0	0.00	0.27	0.82	0.00	0.13
22	-3.6	0.01	0.30	0.99	-0.01	0.14
24	-5.2	0.02	0.33	1.16	-0.02	0.14
26	-6.7	0.03	0.36	1.31	-0.02	0.14
28	-8.2	0.04	0.39	1.44	-0.03	0.13
30	-9.6	0.05	0.42	1.55	-0.04	0.11
32	-10.9	0.06	0.44	1.64	-0.05	0.07
34	-12.0	0.06	0.46	1.70	-0.06	0.03
36	-13.0	0.07	0.48	1.74	-0.06	-0.01
38	-13.9	0.08	0.50	1.76	-0.07	-0.05
40	-14.7	0.09	0.51	1.77	-0.08	-0.08
42	-15.4	0.10	0.52	1.77	-0.09	-0.12
44	-16.0	0.11	0.53	1.76	-0.10	-0.16
46	-16.6	0.12	0.54	1.74	-0.10	-0.20
48	-17.1	0.13	0.54	1.71	-0.11	-0.24
50	-17.6	0.14	0.54	1.68	-0.12	-0.28
52	-18.2	0.15	0.54	1.65	-0.13	-0.32
54	-18.7	0.16	0.54	1.61	-0.14	-0.36
56	-19.2	0.17	0.54	1.58	-0.14	-0.40
58	-19.8	0.17	0.54	1.54	-0.15	-0.44
60	-20.3	0.18	0.54	1.51	-0.16	-0.48
62	-20.8	--	--	--	--	--
64	-21.4	--	--	--	--	--
66	-21.9	--	--	--	--	--
68	-22.4	--	--	--	--	--
70	-23.0	--	--	--	--	--

Summarizing the comparisons, the significant differences between SASS I and SASS II are the following:

1. A 1 to 2 dB offset exists in the 10 m/s NRCS values.
2. The SASS II value for the v-pol α_0 is less than the SASS I value.
3. Large differences occur in α_2.

For the second-order harmonic parameters, a_2 and α_2, a three-way intercomparison can be made

TABLE 3. Wind Speed Differences (m/s) between the SASS I and SASS II Models for Horizontal Polarization

θ_i	Wind Speed, m/s							
	2	3	5	10	15	20	30	2-30
0	0.8	1.2	2.0	4.0	6.0	8.1	12.3	4.9
4	2.3	2.8	3.5	4.4	4.5	4.3	3.0	3.5
20	0.7	0.8	0.7	0.1	-1.0	-2.3	-5.3	-0.9
24	0.8	1.0	1.2	1.2	0.8	0.3	-1.3	0.6
28	0.4	0.6	0.9	1.5	1.9	2.3	2.9	1.5
32	0.2	0.3	0.6	1.2	2.0	2.6	4.0	1.6
36	0.1	0.2	0.5	1.3	2.1	3.0	4.9	1.7
40	0.2	0.4	0.7	1.5	2.4	3.2	4.9	1.9
44	0.4	0.6	0.9	1.8	2.5	3.1	4.2	1.9
48	0.6	0.8	1.2	2.1	2.7	3.3	4.1	2.1
52	0.6	0.8	1.3	2.0	2.5	2.9	3.2	1.9
56	0.4	0.7	1.0	1.6	2.0	2.1	2.0	1.4
60	0.2	0.3	0.5	0.6	0.5	0.2	-0.8	0.2

TABLE 4. Wind Speed Differences (m/s) between the SASS I and SASS II Models for Vertical Polarization

θ_i	Wind Speed, m/s							
	2	3	5	10	15	20	30	2-30
0	0.8	1.2	2.0	4.0	6.0	8.1	12.3	4.9
4	2.2	2.7	3.5	4.3	4.5	4.3	3.0	3.5
20	0.6	0.7	0.6	-0.1	-1.3	-2.7	-6.0	-1.2
24	0.9	1.0	1.1	0.8	0.1	-0.8	-3.2	0.0
28	0.7	0.8	1.0	1.0	0.7	0.3	-1.1	0.5
32	0.6	0.7	0.9	1.0	0.8	0.5	-0.6	0.5
36	0.7	0.8	1.0	1.2	1.0	0.7	-0.4	0.7
40	0.8	1.0	1.2	1.4	1.2	0.7	-0.7	0.8
44	1.0	1.2	1.5	1.6	1.4	0.8	-0.9	0.9
48	1.2	1.4	1.7	1.7	1.3	0.5	-1.7	0.9
52	1.2	1.5	1.7	1.5	0.7	-0.3	-3.1	0.5
56	1.3	1.5	1.6	1.0	-0.1	-1.5	-5.1	-0.2
60	1.1	1.2	1.1	0.0	-1.6	-3.5	-8.1	-1.4

between SASS I, SASS II, and aircraft. For these cases, SASS II is in better agreement with the aircraft than SASS I. This is somewhat surprising because in the original derivation of the NRCS model function, the aircraft data were used to define the directional dependence. However, it appears that subsequent empirical tunings for GOASEX and JASIN substantially distorted this directional dependence. These tunings focused on reducing the wind speed error, rather than the wind direction error.

Tables 1 and 2 list the SASS II model parameters versus incidence angle for horizontal and vertical polarization, respectively. Table entries appear for incidence angles every 2°. The six columns in the table correspond to the following quantities: $10(\alpha_0+\log a_0)$, $a_1+\alpha_1$, $a_2+\alpha_2$, α_0, α_1, α_2. These table values are taken from the solid curve that passes through the SASS II data points in Figures 2 through 13. For the first harmonic parameters, a_1 and α_1, the table values come from (48) and (49). The tables extend only to 60°, except for the first quantity, $10(\alpha_0+\log a_0)$, which has values up to 70°.

For those investigators who use scatterometer wind data, the obvious question is how do the differences in the SASS I and SASS II models affect the retrieval of wind speed and wind direction. In order to answer this question, we did a simulation in which the SASS II model is used to generate the NRCS measurement, and the SASS I model is then used to retrieve the wind speed and direction. For example, given a polarization, incidence angle, wind speed, and wind direction, the SASS II model function generates two NRCS measurements corresponding to the forward and aft antennas. These two simulated measurements are then processed by the standard SASS retrieval algorithm which uses the SASS I GH table. The retrieved wind speed and wind directions are then compared with the true values. In this way we can see how the differences in the NRCS models map into wind speed and wind direction differences. Tables 3 and 4 show the differences in wind speed (retrieved minus true) for horizontal and vertical polarizations. The results are shown for a number of different incidence angles and wind speeds. The table entries are the mean wind speed difference averaged over 36 wind directions ranging from 0° to 350° in 10° steps. The far right column is the mean wind speed difference averaged over all wind directions and all wind speeds for a given incidence angle. The most obvious feature in the two

TABLE 5. Wind Direction Differences (degrees) between the SASS I and SASS II Models for Horizontal Polarization

θ_i	Wind Speed, m/s							
	2	3	5	10	15	20	30	2-30
20	13	11	9	7	6	5	5	9
24	15	13	10	7	6	6	9	10
28	15	13	10	5	7	9	12	10
32	15	13	9	4	8	10	12	11
36	14	12	9	4	8	10	13	11
40	13	11	8	5	9	10	13	10
44	10	8	6	6	9	9	12	9
48	10	9	8	7	8	9	10	9
52	12	12	11	9	8	8	8	10
56	15	13	12	11	10	9	8	11
60	15	13	11	9	7	6	6	10

TABLE 6. Wind Direction Differences (degrees) between the SASS I and SASS II Models for Vertical Polarization

θ_i	Wind Speed, m/s							
	2	3	5	10	15	20	30	2-30
20	15	13	11	8	5	4	5	10
24	17	15	13	9	6	5	5	11
28	16	15	12	8	5	5	8	11
32	15	13	11	7	3	5	9	10
36	13	12	9	5	3	5	9	9
40	11	10	8	3	4	7	10	8
44	9	8	7	2	5	8	11	8
48	9	8	6	3	5	8	12	8
52	8	7	5	4	5	8	11	7
56	7	7	5	4	6	7	11	7
60	7	7	6	3	3	5	9	6

tables is that the wind speed difference is in general a positive value between 1 and 2 m/s. The largest differences occur at nadir where the mean wind speed difference is 4.9 m/s. For incidence angles between 24° and 52°, which correspond to the primary swath for SASS, the average wind speed difference for moderate winds (5 to 15 m/s) is 1.5 m/s for h-pol and 1.1 m/s for v-pol.

Assuming the SASS II model is correct, these results indicate that the wind speeds computed by the SASS I algorithm are biased high by 1 to 2 m/s. Several other pieces of information support this assertion. First, Weller et al. [1983] indicate that the calibration anemometer for JASIN winds is biased about 10% too high. This bias would be absorbed in the SASS I model tuning, and, as a result, the SASS I algorithm would compute winds that are 10% too high. Furthermore, a 1 m/s bias exists between the SASS I winds and the winds obtained from GOASEX [Jones et al., 1982]. Liu [1984] also reports that the SASS I winds are 1 m/s high relative to wind speeds from ship reports. Finally, when compared with Seasat altimeter winds, the SASS I winds at nadir are 3 m/s higher [Wentz et al., 1982]. For the altimeter and SASS comparisons the average wind speed is 8 m/s. At 0° and 8 m/s, Table 3 gives the same 3 m/s bias.

Another interesting feature in Tables 3 and 4 is that over most of the primary swath the h-pol wind speed difference at high winds (20 to 30 m/s) is about 3 to 5 m/s, whereas the v-pol difference is near zero. This says that at high winds, the wind speed retrieved by SASS I using h-pol measurements will be biased high relative to the wind speed retrieved using the v-pol measurements. This is exactly what is observed when SASS modes 3 and 4 are analyzed. In these modes, SASS simultaneously takes horizontal and vertical polarizations measurements. Black et al. [1983] report that for winds between 20 and 30 m/s, the SASS I h-pol winds are typically 5 m/s higher than the v-pol winds.

Tables 5 and 6 show the difference in wind direction for horizontal and vertical polarization. In this case, the table entries correspond to the rms difference averaged over 36 wind directions rather than the mean difference. Because of the harmonic nature of the wind direction dependence, the mean difference caused by the variations in model functions is zero. The smallest rms errors occur for the midrange of incidence angles and wind speeds. In computing the differences we use the alias that is closest in direction to the true wind direction. For the case of four orthogonal aliases, this method of alias selection ensures that the rms error does not exceed 26°, which is the value obtained by assuming a purely random relationship between aliases and the true wind vector. Thus, large differences in the wind direction due to the variation in the NRCS models will be masked by the alias selection procedure.

10. Conclusion

The NRCS model that we derived represents a first-order fit to the 3 months of SASS data. As such, it can be the starting point for more detailed investigations. For example, the model can be compared with observations of very strong winds (20-30 m/s) to determine if there is a departure from the assumed power law relationship. Also, regional variations due to sea-surface temperature, fetch, or other geographically dependent phenomena can be explored by using the model as a baseline. And possibly most important, the model can be extended to include the modification of the 2 cm capillary waves by longer waves.

Finally, we recommend that the model derived herein be used rather than the SASS I model. For the most part, the models are in agreement. However, when there is disagreement, the problem seems to lie with SASS I. To be specific, SASS I has the following drawbacks:

1. For high winds, the winds derived from h-pol do not agree with those derived from v-pol, with the h-pol winds being about 5 m/s higher.
2. In some cases, the wind direction dependence does not agree well with that determined from aircraft.
3. The wind speeds seem to be biased about 1 m/s high.
4. The dependence of some of the parameters on incidence angle is erratic.

The fact that these problems do not occur in the statistically derived NRCS model is very encouraging.

Acknowledgments. This research was made possible by the Canadian Atmospheric and Environment Service (AES) under contract OAJ82-00135, which provided the 3 months of processed SASS data as well as computer support, and by the NASA Oceanic Processes Program under contract NASW-3606, which sponsored the subsequent data analysis. We are grateful to L. McGoldrick at NASA Headquarters for his support of this investigation.

References

Black, P. G., R. C. Gentry, V. J. Cardone, and J. Hawkins, Seasat microwave wind and rain observations in severe tropical and midlatitude storms, Adv. Geophys., in press, 1984.

Bracalente, E. M., D. H. Boggs, W. L. Grantham, and J. L. Sweet, The SASS scattering coefficient σ^0 algorithm, IEEE J. Oceanic Eng., OE-5 (2), 145-154, 1980.

Brooks, C. E. P., C. S. Curst, and N. Karruthers, Upward winds over the world, II, The frequency distribution of winds at a point in free air, Q. J. R. Meteorol. Soc., 72, 55-73, 1946.

Brown, R. A., V. J. Cardone, T. Guymer, J. Hawkins, J. E. Overland, W. J. Pierson, S. Peteherych, J. C. Wilkerson, P. M. Woiceshyn, and M. Wurtele, Surface wind analyses for SEASAT, J. Geophys. Res., 87(C5), 3355-3364, 1982.

Claassen, J. P., A. K. Fung, R. K. Moore, and W. J. Pierson, Jr., Radar sea return and the RADSCAT satellite anemometer, paper presented at IEEE International Conference Engineering in the Ocean Environment, Inst. of Electrical and Electronics Eng., Newport, R. I., 1972.

Cowan, E. W., X-band sea-return measurements, Radiation Lab. Rep. 870, Mass. Inst. of Tech., Cambridge, Mass., 1946.

Daley, J. C., Wind dependence of radar sea return, J. Geophys. Res., 78, 7823, 1973.

Davenport, A. G., The dependence of wind loads on meteorological parameters, in Proceedings of Symposium on Wind Effects on Buildings and Structure, Vol. 1, pp. 20-82, University of Toronto, Ottawa, 1967.

Grant, C. R., and B. S. Yapley, Backscattering from water and land at centimeter and millimeter wavelengths, Proc. IRE, 45, 976, 1957.

Guinard, N. W., J. T. Ransone, Jr., and J. C. Daley, Variation of the NRCS of the sea with increasing roughness, J. Geophys. Res., 76, 1525, 1971.

Jones, W. L., and L. C. Schroeder, Radar backscatter from the ocean: dependence on surface friction velocity, Boundary Layer Meteorol., 13, 133-149, 1978.

Jones, W. L., L. C. Schroeder, D. H. Boggs, E. M. Bracalente, R. A. Brown, G. J. Dome, W. J. Pierson, and F. J. Wentz, The SEASAT-A satellite scatterometer: The geophysical evaluation of remotely sensed wind vectors over the ocean, J. Geophys. Res., 87(C5), 3297-3317, 1982.

Kerr, D. E., Propagation of short radio waves, Dover Publications, New York, 1951.

Kinsman, B. Wind Waves, Their Generation and Propagation on the Ocean Surface, Prentice-Hall, Englewood Cliffs, N. J., 1965.

Liu, W. T., The effect of the variation of sea-surface temperature and atmospheric stability in the estimation of average wind speed by Seasat-SASS, J. Phys. Oceanogr., in press, 1984.

Schroeder, L. C., D. H. Boggs, G. Dome, I. M. Halberstam, W. L. Jones, W. J. Pierson, and F. J. Wentz, The relationsip between wind vector and normalized radar cross section used to derive SEASAT-A satellite scatterometer winds, J. Geophys. Res., 87(C5), 3318-3336, 1982.

U. S. Navy, U. S. Navy Marine Climatic Atlas of the World, vol. 9, Naval Oceanography Command Detachment, Asheville, N. C., May 1981.

Weller, R. A., R. E. Payne, W. G. Large, and W. Zenk, Wind measurements from an array of oceanographic moorings and from F/S Meteor during JASIN 1978, J. Geophys. Res., 88, 9689-9705, 1983.

Wentz, F. J., A two-scale scattering model with application to the JONSWAP '75 aircraft microwave scatterometer experiment, NASA Contr. Rep. 2919, December 1977.

Wentz, F. J., V. J. Cardone, and L. S. Fedor, Intercomparison of wind speeds inferred by the SASS, altimeter, and SMMR, J. Geophys. Res., 87(C5), 3378-3384, 1982.

Young, J. D., and R. K. Moore, Active microwave measurements from space of sea-surface winds, IEEE J. Oceanic Eng., OE2(4), 309-317, 1977.

S. Peteherych, Meteorological Services Research Branch, Atmospheric Environment Service, Downsview, Ontario M3H 5T4.

L. A. Thomas and F. J. Wentz, Remote Sensing Systems, Suite 211, 475 Gate Five Road, Sausalito, CA 94965.

(Received June 13, 1983,
revised September 12, 1983,
accepted November 21, 1983.)